RADIO-SOURCE STRUCTURE IN ASTROMETRIC AND GEODETIC VERY LONG BASELINE INTERFEROMETRY

P. Charlot

Institut Géographique National, 2 Avenue Pasteur, 94160 Saint-Mandé, France

and

Jet Propulsion Laboratory, California Institute of Technology, 4800 Oak Grove Drive, Pasadena, California 91109

Received 1 November 1989; revised 28 December 1989

ABSTRACT

Very Long Baseline Interferometry (VLBI) measurements of the positions of extragalactic radio sources have led to the most precise and stable celestial reference frame available to date. Generally, these radio sources exhibit spatially extended structures that are variable in both time and frequency on the milliarcsecond scale. Such radio-source structures set limits on possible improvements of the VLBI celestial reference frame and on its use for geodynamic and deep space navigation VLBI measurements. We present a study of the effects of radio-source structures in the delay and delay rate, which are the fundamental observables measured by VLBI for astrometric and geodetic applications. This study includes the theoretical formulation to model these effects, simulations for a simple two-component source, and analysis of real astrometric VLBI data acquired on the complex radio source NRAO140. For this source, the structure corrections have been calculated with maps produced by three different VLBI imaging techniques: the hybrid-CLEAN algorithm, the maximum entropy method, and model fitting. We compare the structure corrections calculated with the three brightness distributions to the actual data by forming the closure delays and delay rates. In this comparison, the measured closure delays and delay rates are from the same dataset as the amplitudes and closure phases used to map NRAO140. We conclude that the CLEAN map produces the most accurate structure corrections in this example.

I. INTRODUCTION

In recent years, high-quality VLBI observations of extragalactic radio sources have resulted in determination of baseline vector components between radio telescopes and source positions with centimeter and milliarcsecond (mas) level accuracies, respectively (Ma, Himwich, and Caprette 1989; Sovers *et al.* 1989; Carter, Robertson, and Fallon 1989). The estimation of the geodetic and astrometric parameters is based on the analysis of Band Width Synthesis (BWS) delays and delay rates measured by the VLBI technique. The formal precision of a single BWS delay measurement is now at the 10 picosecond (ps) level with the Mark III wide-band data acquisition system (Rogers *et al.* 1983), but the root-mean-square of typical post-fit BWS delay residuals is about 50 ps in such analysis (Ma, Ryan, and Caprette 1989; Sovers 1989). Hence, significant improvements of the theoretical model used to compute the BWS delays are necessary to avoid systematic errors larger than the measurement uncertainties, and therefore to enhance the quality of the terrestrial and celestial reference frames built from VLBI data. A long-term goal is to include in the model all the phenomena that can cause effects at the 10 ps level.

A known source of error in modeling the BWS delay is related to stochastic propagation effects, especially those due to the wet component of the troposphere, which presently cannot be determined to better than a few centimeters of path delay from meteorological data (Treuhaft and Lanyi 1987). However, recent advances both in calibration [by the use of Water Vapor Radiometers (WVR)] and in data processing (e.g., Kalman filtering, see Davis, Herring, and Shapiro 1988) are promising. A second cause of error is the structure of the radio sources. At the milliarcsecond level, most of these sources exhibit time–variable extended structure and therefore are not ideal targets for ultraprecise geodesy and astrometry unless this structure can be accounted for. Radio-source structure effects were first mentioned by Coates *et al.* (1975), and were then studied by Cotton (1979) and Thomas (1980). Recently, several authors pointed out the importance of these effects in geodesy and astrometry (Charlot, Lestrade, and Boucher 1988; Ulvestad 1988; Campbell, Schuh, and Zeppenfeld 1988; Tang and Rönnäng 1988). While the propagation effects are stochastic, the contribution due to source structure in BWS delays and delay rates is deterministic. It can be calculated when brightness distributions of radio sources are known. VLBI amplitude and closure phase observables and various imaging techniques (e.g., hybrid-mapping algorithms, see Readhead and Wilkinson 1978; Cornwell and Wilkinson 1981) can produce such brightness distributions. It has recently been shown that the data of a typical geodetic VLBI experiment of the Crustal Dynamics Program are sufficient by themselves to map all the sources observed, although the *u-v* coverage is generally sparse in this type of experiment (Charlot 1990).

We have implemented an algorithm to calculate source structure corrections for BWS delays and delay rates in order to refer the position of each source to a specific feature of its morphology, for example, its core. The algorithm used is first described. Then, simulations in the case of a two-component source are shown. These simulations are useful to estimate the magnitude of the structure corrections and to set limits on the quality of the maps required to properly model these effects. Finally, results for the complex radio source NRAO140 are presented. This source was observed for calibration in the course of an experiment on radio stars with a six-station array in July 1983. The amplitudes and closure phases were used to produce maps of NRAO140 with three different methods: the hybrid-CLEAN algorithm, the maximum entropy method, and model fitting (for a re-

view of these methods, see, e.g., Pearson and Readhead 1984). These maps were then used to derive structure corrections for the delays and delay rates of NRAO140 measured during the same experiment. These corrections are significant and depend on the imaging technique adopted at some level since the brightness distributions produced by the three techniques are slightly different. We discuss the degree of agreement between the three sets of calculated structure corrections and the real data by forming the closure delays and delay rates.

II. THEORY

The complex visibility function V of a spatially extended source, measured by an interferometer with baseline vector $\mathbf{B}$ is

$$V(\mathbf{B},\omega,t) = \iint_{\Omega_s} I(P,\omega,t)\exp\left(-\frac{2\pi i}{\lambda}\mathbf{B}\cdot\mathbf{k}_P\right)d\Omega, \quad (1)$$

where $I(P,\omega,t)$ is the intensity of the brightness distribution of the source at the point P on the sky for the frequency $\omega = 2\pi c/\lambda$ and the time t, $\mathbf{k}_P$ is a unit vector pointing toward P from the Earth's center, and $d\Omega$ is a differential solid angle for integration over the extended source of solid angle Ω_s. By adopting a reference point P_0 within the source, $\mathbf{k}_P$ can be written as

$$\mathbf{k}_P = \mathbf{k}_{P_0} + \mathbf{P}_0\mathbf{P},$$

where $\mathbf{P}_0\mathbf{P}$ (in the plane of the sky) and $\mathbf{k}_{P_0}$ are orthogonal since VLBI structures extend over a very narrow portion of the sky. The visibility function is then the product of two complex numbers:

$$V(\mathbf{B},\omega,t) = \exp\left(-\frac{2\pi i}{\lambda}\mathbf{B}\cdot\mathbf{k}_{P_0}\right)$$
$$\times \iint_{\Omega_s} I(P,\omega,t)\exp\left(-\frac{2\pi i}{\lambda}\mathbf{B}\cdot\mathbf{P}_0\mathbf{P}\right)d\Omega, \quad (2)$$

which can also be expressed by

$$V = A\exp[i(\phi_g + \phi_s)]$$
$$= A\exp(i\phi_t), \quad (3)$$

with

$$A = \left|\iint_{\Omega_s} I(P,\omega,t)\exp\left(-\frac{2\pi i}{\lambda}\mathbf{B}\cdot\mathbf{P}_0\mathbf{P}\right)d\Omega\right|, \quad (4)$$

$$\phi_s = \arg\left[\iint_{\Omega_s} I(P,\omega,t)\exp\left(-\frac{2\pi i}{\lambda}\mathbf{B}\cdot\mathbf{P}_0\mathbf{P}\right)d\Omega\right], \quad (5)$$

$$\phi_g = -(2\pi/\lambda)\mathbf{B}\cdot\mathbf{k}_{P_0}. \quad (6)$$

A is the amplitude observed by the interferometer, ϕ_g is the geometric phase for the direction $\mathbf{k}_{P_0}$, ϕ_s is the additional structure phase for the brightness distribution $I(P,\omega,t)$ and the reference point P_0, and $\phi_t = \phi_g + \phi_s$ is the total phase.

The VLBI group delay and delay rate observables used in astrometry are defined by the partial derivatives of the total phase with respect to frequency and time. For an extended source, they can be written as

$$\tau = \frac{\partial\phi_t}{\partial\omega} = \frac{\partial\phi_g}{\partial\omega} + \frac{\partial\phi_s}{\partial\omega}$$
$$= -(1/c)\mathbf{B}\cdot\mathbf{k}_{P_0} + \tau_s \quad (7)$$

and

$$\dot{\tau} = \frac{1}{\omega}\frac{\partial\phi_t}{\partial t} = \frac{1}{\omega}\frac{\partial\phi_g}{\partial t} + \frac{1}{\omega}\frac{\partial\phi_s}{\partial t}$$
$$= -\frac{1}{c}\frac{d}{dt}(\mathbf{B}\cdot\mathbf{k}_{P_0}) + \dot{\tau}_s, \quad (8)$$

where τ_s and $\dot{\tau}_s$ are source structure effects. Thus, the absolute VLBI position determined in astrometry is the position of the adopted reference point P_0 if structure effects are accounted for in the modeled delays and delay rates. The choice of the reference point is critical for the stability of the celestial reference frame. This point should be a specific feature of the source morphology that is easily recognizable over time and frequency. In practice, no general rule can be established and the choice should be made on a source by source basis. However, most of the radio sources used in astrometry have a compact core that partially fulfills the above requirements and which therefore can be adopted as the reference point.

Since brightness distributions are generally referred to a local coordinate frame in the plane of the sky near the source, in practice it is convenient to introduce an arbitrary origin $\mathbf{O}$ in the expression of ϕ_s so that $\mathbf{P}_0\mathbf{P} = \mathbf{OP} - \mathbf{OP}_0$. Adopting the mathematical form used by Thomas (1980), ϕ_s can be written as

$$\phi_s = \frac{2\pi}{\lambda}\mathbf{B}\cdot\mathbf{OP}_0 + \tan^{-1}\left(\frac{-Z_s}{Z_c}\right), \quad (9)$$

where Z_c and Z_s are the following real numbers:

$$Z_c = \iint_{\Omega_s} I(P,\omega,t)\cos\left(\frac{2\pi}{\lambda}\mathbf{B}\cdot\mathbf{OP}\right)d\Omega, \quad (10)$$

$$Z_s = \iint_{\Omega_s} I(P,\omega,t)\sin\left(\frac{2\pi}{\lambda}\mathbf{B}\cdot\mathbf{OP}\right)d\Omega. \quad (11)$$

Then τ_s and $\dot{\tau}_s$ are

$$\tau_s = \frac{1}{c}\mathbf{B}\cdot\mathbf{OP}_0 + \left(Z_s\frac{\partial Z_c}{\partial\omega} - Z_c\frac{\partial Z_s}{\partial\omega}\right)\Big/(Z_c^2 + Z_s^2), \quad (12)$$

$$\dot{\tau}_s = \frac{1}{c}\frac{d}{dt}(\mathbf{B}\cdot\mathbf{OP}_0) + \frac{1}{\omega}\left(Z_s\frac{\partial Z_c}{\partial t} - Z_c\frac{\partial Z_s}{\partial t}\right)\Big/(Z_c^2 + Z_s^2). \quad (13)$$

Complete analytical derivations of the terms depending on Z_c and Z_s in Eqs. (12) and (13) are given in Thomas (1980). In practice, only the expressions of Z_c and Z_s [Eqs. (10) and (11)] need to be derived to calculate the BWS delay and delay rate structure effects (see Sec. III). The computation of Z_c and Z_s requires a representation of the brightness distribution $I(P,\omega,t)$. There are three cases of practical importance: a finite number of delta functions (hybrid map obtained with the CLEAN algorithm), a two-dimensional piecewise-constant brightness distribution (hybrid map obtained with the maximum entropy method), and a finite number of Gaussian functions (model fitted to the

data). Hereafter, we simplify the notation $I(P,\omega,t)$ by using $I(P)$ only.

a) Delta Functions

In the case of n delta functions, the brightness distribution is given by

$$I(P) = \sum_{k=1}^{n} S_k \delta(\mathbf{OP} - \mathbf{OP}_k), \tag{14}$$

where P_k is the position of the kth delta function and S_k is its flux density. Then, the expressions of Z_c and Z_s [Eqs. (10) and (11)] become numerical sums:

$$Z_c = \sum_{k=1}^{n} S_k \cos\left(\frac{2\pi}{\lambda}\mathbf{B}{\cdot}\mathbf{OP}_k\right), \tag{15}$$

$$Z_s = \sum_{k=1}^{n} S_k \sin\left(\frac{2\pi}{\lambda}\mathbf{B}{\cdot}\mathbf{OP}_k\right). \tag{16}$$

b) Piecewise-Constant Distribution

A two-dimensional piecewise-constant brightness distribution is composed of a finite number of similar symmetric functions. In such a case, the structure effects depend on the positions and intensities of these functions, but not on their shape; for the calculation of the structure effects, each pixel can be replaced by a delta function located at its center with a flux density equal to that of the pixel (Fujishita 1983). Thus, Eqs. (15) and (16) apply also.

c) Gaussian Functions

For Gaussian functions of different size and orientation, a complete derivation has been carried out in Charlot (1989) and gives

$$Z_c = \sum_{k=1}^{n} \left[S_k e^{-2\pi^2(a_k^2 U_k^2 + b_k^2 V_k^2)} \cos\left(\frac{2\pi}{\lambda}\mathbf{B}{\cdot}\mathbf{OP}_k\right)\right], \tag{17}$$

$$Z_s = \sum_{k=1}^{n} \left[S_k e^{-2\pi^2(a_k^2 U_k^2 + b_k^2 V_k^2)} \sin\left(\frac{2\pi}{\lambda}\mathbf{B}{\cdot}\mathbf{OP}_k\right)\right], \tag{18}$$

with

$$a_k = \frac{\mathrm{FWHM}_k \, (\text{major axis})}{2\sqrt{2\log 2}},$$

$$b_k = \frac{\mathrm{FWHM}_k \, (\text{minor axis})}{2\sqrt{2\log 2}},$$

and

$$U_k = u \sin\psi_k + v \cos\psi_k,$$

$$V_k = -u \cos\psi_k + v \sin\psi_k,$$

where u and v are the coordinates (expressed in number of wavelengths) of the baseline vector projected on the plane of the sky along the East–West and North–South directions, P_k is the position of the kth Gaussian function, ψ_k is the position angle of its major axis, counted from the North and positive counterclockwise, and S_k is its flux density.

III. CASE OF A TWO-COMPONENT MODEL

The study of a simple two-component model is useful to estimate the magnitude and time variations of the structure effects for most of the sources, since many extended sources can crudely be represented by such a model. Hereafter, a

model composed of two delta functions with flux densities S_1 and S_2 ($S_2 < S_1$), and located in the plane of the sky at P_1 and P_2, is considered. To simplify the calculations, the axis joining the two components is chosen parallel to the u axis, P_1 is chosen at the origin O of the local coordinate frame, and the reference point P_0 is chosen at the barycenter of the brightness distribution of the model ($\mathbf{P}_1\mathbf{P}_0 = [S_2/(S_1 + S_2)]\mathbf{P}_1\mathbf{P}_2$). It is to be noted that this latter choice would not be appropriate for analysis of actual VLBI data spanning several years, since the barycenter of the brightness distribution of a source is likely to move with time.

a) Analytical Formulas

Source structure effects for a two-component model can be written as functions of $K = S_2/S_1$ and $R = (\mathbf{B}/\lambda){\cdot}\mathbf{P}_1\mathbf{P}_2$. R is the ratio between the separation of the two components and the projected interferometer fringe spacing along the source axis. In this case, the structure phase ϕ_s, derived from Eqs. (9), (15), and (16), is

$$\phi_s = \frac{2\pi K}{1 + K}R + \tan^{-1}\left(\frac{-K\sin(2\pi R)}{1 + K\cos(2\pi R)}\right). \tag{19}$$

Expressions of the structure effects τ_s and $\dot{\tau}_s$ are obtained analytically by taking the partial derivatives of ϕ_s with respect to frequency and time [Eqs. (12) and (13)]. For this derivation, the flux densities of the two components are assumed frequency and time independent. Then

$$\tau_s = \frac{2\pi K(1 - K)}{\omega(1 + K)}\frac{[1 - \cos(2\pi R)]R}{K^2 + 2K\cos(2\pi R) + 1} \tag{20}$$

and

$$\dot{\tau}_s = \frac{2\pi K(1 - K)}{\omega(1 + K)}\frac{[1 - \cos(2\pi R)]\dot{R}}{K^2 + 2K\cos(2\pi R) + 1}. \tag{21}$$

τ_s and $\dot{\tau}_s$ depend on the orientation of the sky projection of the baseline relative to the main features of the source morphology. Maxima of τ_s are for $R = 0.5 + n + \epsilon$, where n is an integer, and ϵ is small compared to $0.5 + n$ (Thomas 1980; Charlot 1989). A good approximation of the intensities of these maxima is obtained for $R = 0.5 + n$. Thus,

$$(\tau_s)_{\max} \sim [4\pi K/\omega(1 - K^2)](0.5 + n), \tag{22}$$

$(\tau_s)_{\max}$ is very large when K is close to unity ($S_1 \sim S_2$) and can theoretically reach an infinite value when $K = 1(S_1 = S_2)$. In Eq. (22), it is also noticeable that $(\tau_s)_{\max}$ is proportional to $(0.5 + n)$ so that it is larger when the separation $|\mathbf{P}_1\mathbf{P}_2|$ between the two components is a higher multiple of the projected interferometer fringe spacing along the source axis. Maxima of $\dot{\tau}_s$ depend on $\dot{R}$, and therefore on the geometry of the problem. An upper limit of the intensities of these maxima is

$$(\dot{\tau}_s)_{\max} \leqslant [4\pi K/\omega(1 - K^2)]\Theta R_{\max}, \tag{23}$$

where Θ is the angular velocity of the Earth, and $R_{\max}$ is the maximum possible value of R for the geometry considered ($R_{\max} = (|\mathbf{B}|/\lambda){\cdot}|\mathbf{P}_1\mathbf{P}_2|$).

b) Numerical Simulation

We present now a numerical simulation for an equatorial baseline and a zero declination source, which simplifies the calculation and interpretation. For this geometry, R varies between $-R_{\max}$ and $+R_{\max}$ over 24 hr. Figures 1(a)–
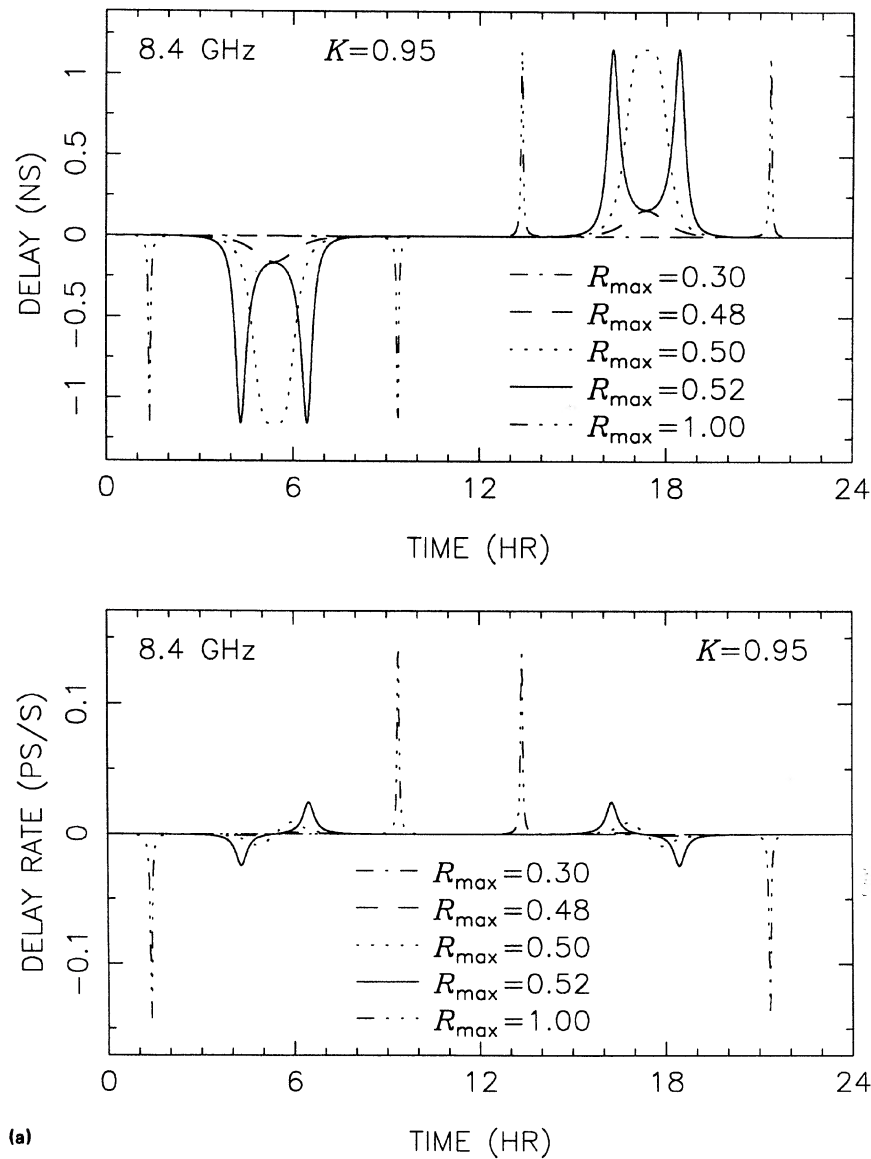
FIG. 1. Hour angle variations of VLBI group delay and phase delay rate at 8.4 GHz due to the structure of an ideal two-component radio source with a frequency-independent flux-density ratio K. The parameter R_{max} of the curves is the ratio of the sky separation between the two components and the maximum projected interferometer fringe spacing along the source axis. The geometry has been simplified by taking an equatorial baseline and a zero declination source. (a) $K = 0.95$; (b) $K = 0.80$; (c) $K = 0.50$.
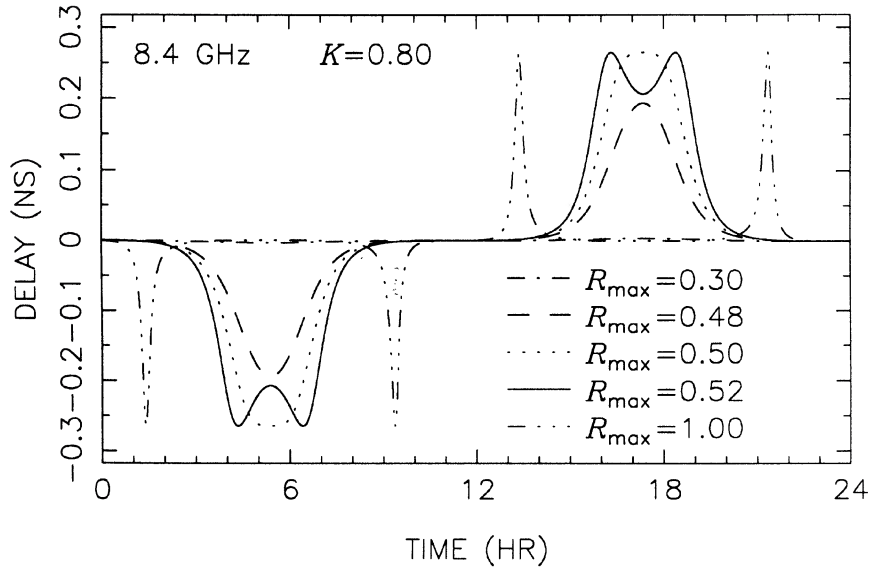
FIG. 1. (continued)
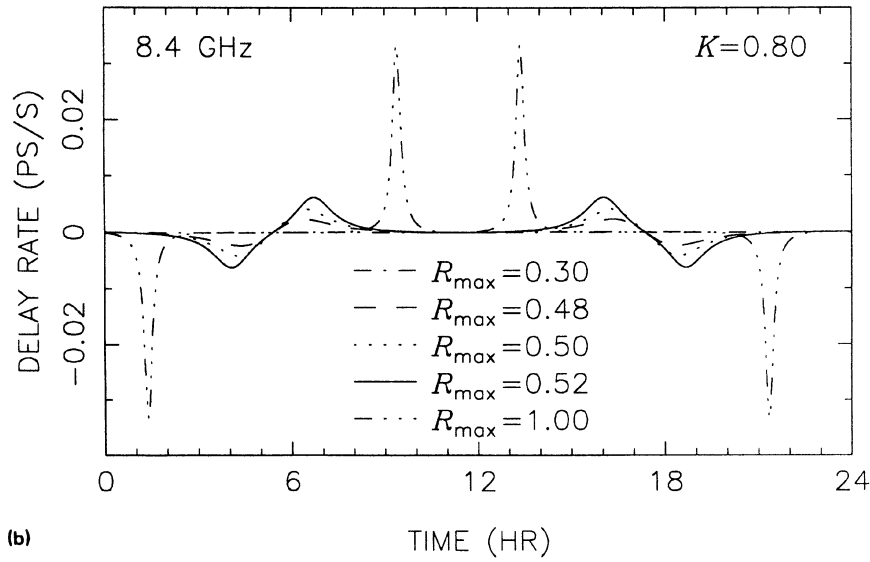
(b)
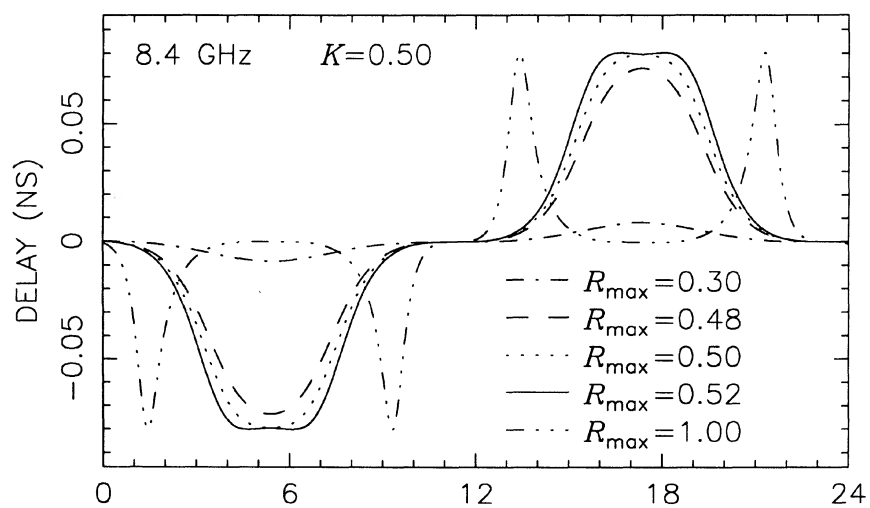
FIG. 1. (continued)
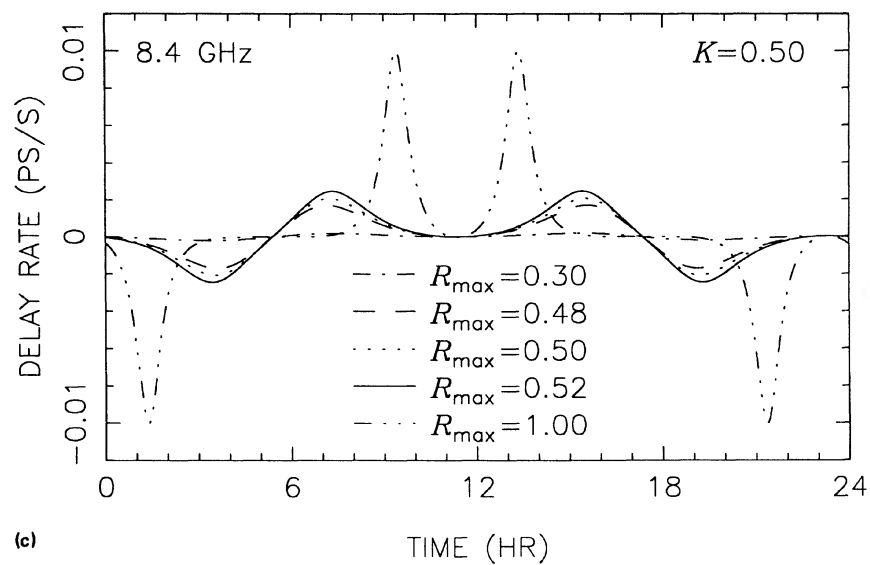
(c)

1(c) show the structure effects τ_s and $\dot{\tau}_s$ at 8.4 GHz for $K = 0.95$, $K = 0.80$, and $K = 0.50$ ($K = S_2/S_1$). There are five curves in each plot, corresponding to values of $R_{\max}$ between 0.3 and 1.0. For a typical component separation (e.g., 1 mas) and an intercontinental baseline, one has $0.5 < R_{\max} < 1.5$. In this case, the u-v track of the baseline crosses the straight lines $R = \pm 0.5$ four times, giving rise to the four peaks seen for τ_s and $\dot{\tau}_s$ in Figs. 1(a)–1(c). Had $R_{\max}$ been larger than 1.5 (the case of a source with a component separation larger than 2 mas), the u-v track of the baseline would have also crossed the straight lines $R = \pm 1.5$, and τ_s and $\dot{\tau}_s$ would have exhibited four additional peaks with higher intensity (Charlot 1989). When $R_{\max} \sim 0.5$ (see curves plotted for $R_{\max} = 0.48, 0.50, 0.52$ in Fig. 1), each pair of adjacent peaks blends into one for τ_s, and structure effects last over a longer time period than when $R_{\max} > 0.5$. It is also noticeable that the peaks of τ_s and $\dot{\tau}_s$ widen when K lessens as shown from Figs. 1(a) to 1(c): for $R_{\max} = 1$, the width of the peaks at 0.1 peak height is ~ 15 min if $K = 0.95$, ~ 1 h if $K = 0.80$, and $\sim 2^h 30^m$ if $K = 0.50$. The peak intensities of τ_s in these figures are given by Eq. (22) as 1.15 ns if $K = 0.95$, 0.26 ns if $K = 0.80$, and 0.080 ns if $K = 0.50$. In addition, a maximum effect of 12 ps was found for $K = 0.10$. For the purpose of modeling the delay at the 10 ps level, it is therefore necessary to account for structure effects of sources with $K \geqslant 0.1$ when $0.5 < |R_{\max}| < 1.5$ if their structures are reducible to a two-component model. A large number of the radio sources observed in astrometric and geodetic VLBI programs fall into this category.

Figure 1(a) ($K = 0.95$) shows that the behavior of the structure effect τ_s as a function of $R_{\max}$ undergoes a sharp transition from two separated peaks to a plateau when $R_{\max}$ is in the vicinity of 0.5 (see curves plotted for $R_{\max} = 0.48, 0.50, 0.52$). In this case, a 4% variation of $R_{\max}$ (i.e., by 0.02) due to a slight change in the geometry of the interferometer or in the separation $|\mathbf{P}_1\mathbf{P}_2|$ causes a variation of about 1 ns in τ_s. Hence a 4% precision on the separation $|\mathbf{P}_1\mathbf{P}_2|$ between the two nearly equal components of the source is not sufficient to properly model the structure effect τ_s. When $R_{\max}$ is not in the vicinity of 0.5 (e.g., $R_{\max} = 1$), a small variation of this parameter produces only a slight shift in time of the peaks but large differences in the magnitude of the effect τ_s because of the sharpness of the peaks. In fact, it can be shown that for any value of $R_{\max}$ between 0.5 and 1.5, a precision of about 0.02% on the separation $|\mathbf{P}_1\mathbf{P}_2|$ is necessary to model the structure effect τ_s at the 10 ps level when $K = 0.95$ ($K = S_2/S_1$). Such a precision is not presently obtainable in VLBI maps. Thus, it is unlikely that structure effects for nearly equal two-component sources could be properly modeled at the epochs of the peaks, and any data acquired during these periods should be eliminated. Figure 1(c) ($K = 0.50$) shows that the transition from $R_{\max} = 0.48$ to $R_{\max} = 0.50$ and 0.52 is smoother when K is lower. In this case, the separation $|\mathbf{P}_1\mathbf{P}_2|$ needs to be known only to about 5% to model the structure effect τ_s at the 10 ps level; hence, this effect could be properly predicted from hybrid maps.

c) Effects of Large Bandwidth and Finite Integration Time

Additional simulations for VLBI observations acquired over large bandwidths like those conducted by the Crustal Dynamics Program (bandwidth of 360 MHz at 8.4 GHz and 85 MHz at 2.3 GHz) are presented in Charlot (1989). They indicate that the structure effect τ_s derived for the group

delay at a single frequency [Eq. (12)] is not appropriate for the BWS delay produced with several 2 MHz bands spanning 360 MHz at 8.4 GHz, because the structure phase ϕ_s is not linear over such a bandwidth. For example, when $K = 0.95$, structure BWS delay maxima are 25% lower than those calculated for the group delay at a single frequency corresponding to the mean value of the eight frequency channels used by the Crustal Dynamics Program at 8.4 GHz. At the correlator, the BWS delay observable is obtained by fitting a slope to the residual phases measured in those narrowband channels. It is necessary to proceed in the same way for calculating accurately the contribution of the structure effect to this observable. Thus, the BWS delay structure correction should be determined as the slope of a straight line fitted to the individual structure phases calculated for each frequency channel used during the observations. In addition, spectral indices of source components can be accounted for by assigning a different brightness distribution to each frequency channel when calculating the structure phases (see discussion below).

Similarly, it is also worth noting that the delay rate observable is determined at the correlator by fitting a slope to the residual phases over time so that the contribution of the structure effect in the delay rate is not equivalent to the time derivative $\dot{\tau}_s$ of Eq. (13). However, in our analysis it is not possible *to duplicate exactly* the computation scheme used at the correlator where unknown uneven weights for the 1 s integration periods have entered into the fit to determine the delay rate. In practice, the following approximate formula is adopted to calculate $\dot{\tau}_s$

$$\dot{\tau}_s \sim \frac{1}{\omega} \left(\frac{\phi_s(t_2) - \phi_s(t_1)}{t_{\mathrm{int}}} \right), \tag{24}$$

with

$$t_1 = t_0 - (t_{\mathrm{int}}/2),$$
$$t_2 = t_0 + (t_{\mathrm{int}}/2),$$

and where t_0 is the mean epoch of the observation, and t_{int} is the integration time.

d) Source Spectral Index Effect

In our simulation, the possible frequency dependence of the flux densities of the two components has not been accounted for. This frequency dependence induces an additional term in the structure delay that is proportional to the spectral index difference of the two components for the ideal source considered here. Although this is often overlooked, this term does not depend on the bandwidth spanned in the observations and exists both in the group delay and the BWS delay. For the group delay, the following term must be added to τ_s of Eq. (20) (Thomas 1980; Charlot 1989):

$$\Delta I_\omega = \frac{K(\alpha_1 - \alpha_2)}{\omega} \frac{\sin(2\pi R)}{K^2 + 2K\cos(2\pi R) + 1}, \tag{25}$$

where α_1 and α_2 are the spectral indices of the two components [$S_1(\omega) \propto \omega^{\alpha_1}$ and $S_2(\omega) \propto \omega^{\alpha_2}$]. Extrema of ΔI_ω are $\pm (\alpha_1 - \alpha_2)K/[\omega(1 - K^2)]$ (Charlot 1989), which are ± 185 ps for $K = 0.95$ and ± 13 ps for $K = 0.50$ at 8.4 GHz, assuming a physically common spectral index difference $\alpha_1 - \alpha_2 = 1$ (e.g., Kellermann and Pauliny-Toth 1981). Thus, the frequency dependence of the two components should be accounted for if $K \geqslant 0.5$ for modeling the structure delay at the 10 ps level in this case ($\alpha_1 - \alpha_2 = 1$).

Figure 2 shows the contribution due to ΔI_ω in the group delay over a 24 hr period for various values of R_{max} ($0.3 \leqslant R_{max} \leqslant 1$), assuming $\omega/2\pi = 8.4$ GHz, $K = 0.95$, and $\alpha_1 - \alpha_2 = 1$. This effect corresponds to about 15% of the main term represented in Fig. 1(a) and is to be considered for real observations. The contribution due to ΔI_ω can even be larger if $\alpha_1 - \alpha_2 > 1$. For example, there is a spectral index difference of ~ 2.5 between two nearly equal components in the core region of 3C 454.3 at epoch 1985.37 (Charlot 1990). In this case, the frequency dependence of the flux densities could cause a 40% error if ignored when calculating the structure delay. It is to be noted that $\alpha_1 - \alpha_2$ can be as large as 5 for an ideal synchrotron source consisting of an optically thick one-component core ($\alpha_1 = +2.5$) and an optically thin ejecta with electron energy index $\delta = 6(\alpha_2 = -2.5)$ (Dulk 1985). In Fig. 2, it is also noticeable that the shapes of the curves change very briskly from $R_{max} = 0.48$ to $R_{max} = 0.50$ and 0.52. As for the main structure effect [Eq. (20)], it is likely that ΔI_ω cannot be properly modeled in this case unless the separation of the two components is known to a high accuracy.

IV. CASE OF THE RADIO SOURCE NRAO140

VLBI astrometric data obtained on the complex radio source NRAO140 serve as a stringent example to check that both mapping and calculating structure corrections are possible at some level for this complex source.

a) Brightness Distribution of NRAO140

NRAO140 was observed as a calibrator at 5 GHz during an experiment on radio stars in July 1983 (Lestrade et al. 1985) with a six-station VLB array (Effelsberg, Haystack, Greenbank, Fort Davis, phased VLA, Owens Valley). The data were sufficient to study the structure of this source by three different methods: the hybrid-CLEAN algorithm, the maximum entropy method (MEM), and model fitting (for a review of these methods, see, e.g., Pearson and Readhead 1984). Our maps and model are presented and discussed in Charlot, Hough, and Lestrade (1989), hereafter referred to as CHL89. Only the CLEAN map has been reproduced in Fig. 3. The structure of NRAO140 is of the core-jet type and consists of four components, two of which (A and B) have nearly equal intensities, while the two others (C and D) have comparatively low intensities (see Fig. 3). Superluminal motion with $v \sim 4c$ ($\mu = 0.12$ mas/yr) was observed at 10.7 GHz between A and B by Marscher and Broderick (1982). In addition, these authors distinguished two subcomponents in component A (Marscher and Broderick 1985), and Marscher (1988) reported furthermore that these two subcomponents exhibit a superluminal motion similar to the one between A and B.

For the calculation of the structure effects on the BWS delays and delay rates of NRAO140, component B was selected as the reference point. This feature was chosen because it is well separated from the other components and relatively unresolved, whereas the core is blended with the innermost jet component and elongated at the epoch of our observations. However, for long-term astrometric solutions, component B should not be selected as the reference point because it moves away from the core which is generally thought to be stable in extragalactic radio sources. This core stability has been demonstrated at the level of 20 microarcsec/yr for the quasars 3C 345 and NRAO512 (Bartel et al. 1986). The difficulty in choosing the proper reference point in NRAO140 is an example of the complexity of future ultraprecise VLBI astrometry.
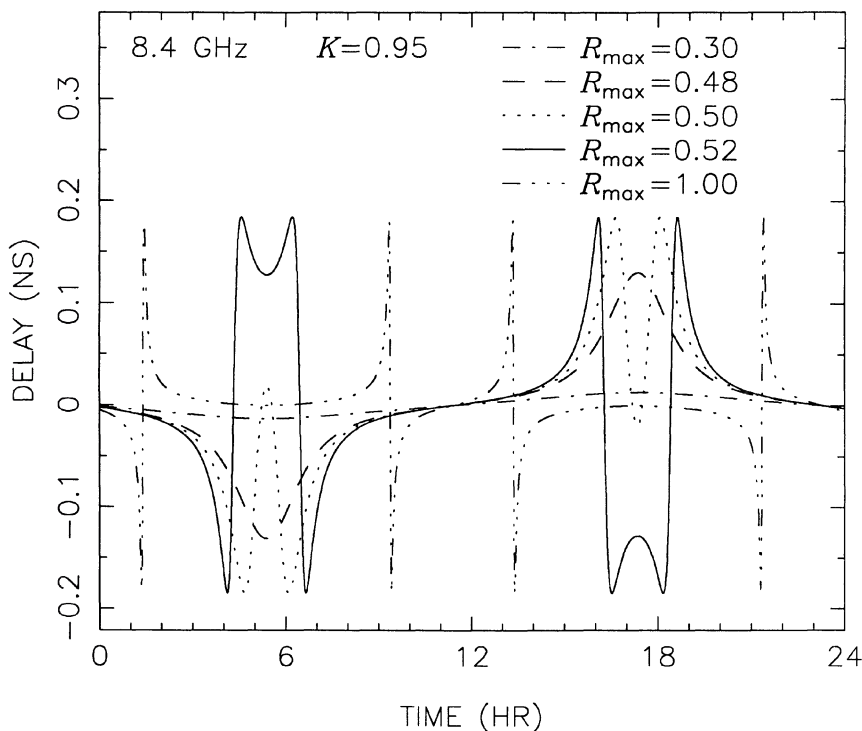
FIG. 2. Hour angle variations of VLBI group delay at 8.4 GHz due to the frequency dependence of the brightness distribution of an ideal two-component radio source with a flux-density ratio $K \sim 0.95$ and a spectral index difference $\alpha_1 - \alpha_2 = 1$. The parameter R_{max} of the curves is the ratio of the sky separation between the two components and the maximum projected interferometer fringe spacing along the source axis. The geometry has been simplified by taking an equatorial baseline and a zero declination source.
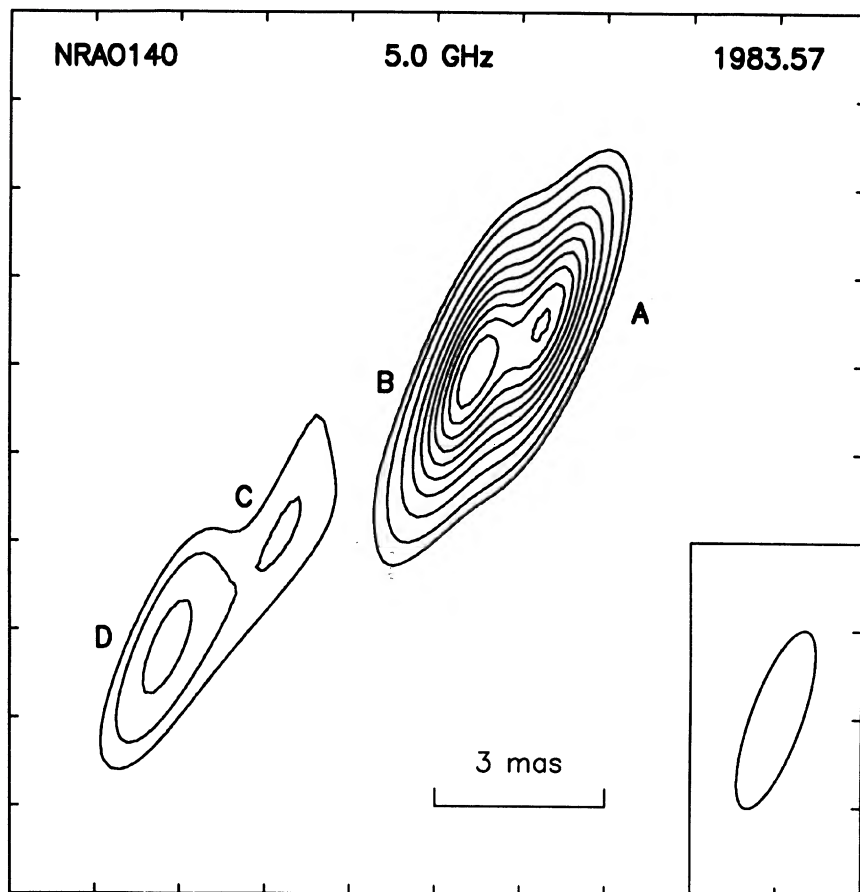
FIG. 3. 5 GHz hybrid-CLEAN map of NRAO140 at epoch 1983.57. Contour levels are 8%, 12%, 20%, 30%, 40%, 50%, 60%, 70%, 80%, and 90% of the peak brightness.

b) Comparison of the Structure Effects Calculated with the CLEAN Map, the MEM Map, and the Four-Component Model of NRAO140

The CLEAN map, the MEM map, and the four-component model of CHL89 have been used to calculate structure effects for NRAO140 at 5 GHz. For this calculation, all pixels with intensities under the dynamic range of our MEM map ($\sim 8\%$ of the peak brightness) and all low-intensity CLEAN components that are obviously not part of the four components A, B, C, and D, have been eliminated. Figures 4(a) and 4(b) show the structure effects derived from the three brightness representations for the intercontinental baselines Effelsberg–Haystack and Effelsberg–VLA during the experiment. A significant peak both in delay and delay rate appears for each baseline during this period. In Fig. 5, the u-v plane of NRAO140 is plotted in order to compare the epochs of the peaks with the u-v coordinates of the projected baselines. It is clear that the peaks appear when the u-v tracks cross the straight line $R = 0.5$ orthogonal to the jet structure of the source (here R is the ratio between the separation of the components A and B and the projected interferometer fringe spacing along the source axis, see Sec. III). Similar structure effects have been found for the other intercontinental baselines. For continental U.S. baselines, the effects are less spiky and smaller than 0.2 ns. This is because the u-v tracks of these baselines do not cross the straight line $R = 0.5$ (see Fig. 5).

Comparing Figs. 4(a) and 4(b) shows that the peak intensities derived from the three different representations of the brightness distribution are roughly the same for the baseline Effelsberg–Haystack, whereas for the baseline Effelsberg–VLA the peak intensity derived from the four-component model is four times higher than those derived from the CLEAN and MEM maps. By examining the u-v visibility contours produced by this model, it is noticeable that the u-v track of the baseline Effelsberg–VLA at the epoch of the peak goes very close to a point of null visibility. Moreover, by changing slightly the Gaussian parameters of the model consistently with their uncertainties, it is possible to shift this null visibility point exactly on the u-v track of the baseline, which results in infinite structure corrections. Thus, the Gaussian component representation is not accurate enough to properly model the structure effects in this region. The peak intensities produced by the CLEAN and MEM maps on the baseline Effelsberg–VLA [Fig. 4(b)] are also significantly different (0.53 and 0.77 ns, respectively). Such a difference can be accounted for by a variation of 5% of the intensity ratio K of the components A and B as indicated by Eq. (22), if the structure of NRAO140 is reduced to two delta function components. This difference is consistent with the uncertainties quoted for the flux densities of components A and B in CHL89 ($\sim 7\%$ for A and $\sim 5\%$ for B).

In Fig. 4, it is also noticeable that the peaks produced by the three representations are not exactly time registered. For example, on the baseline Effelsberg-VLA, the peak pro-
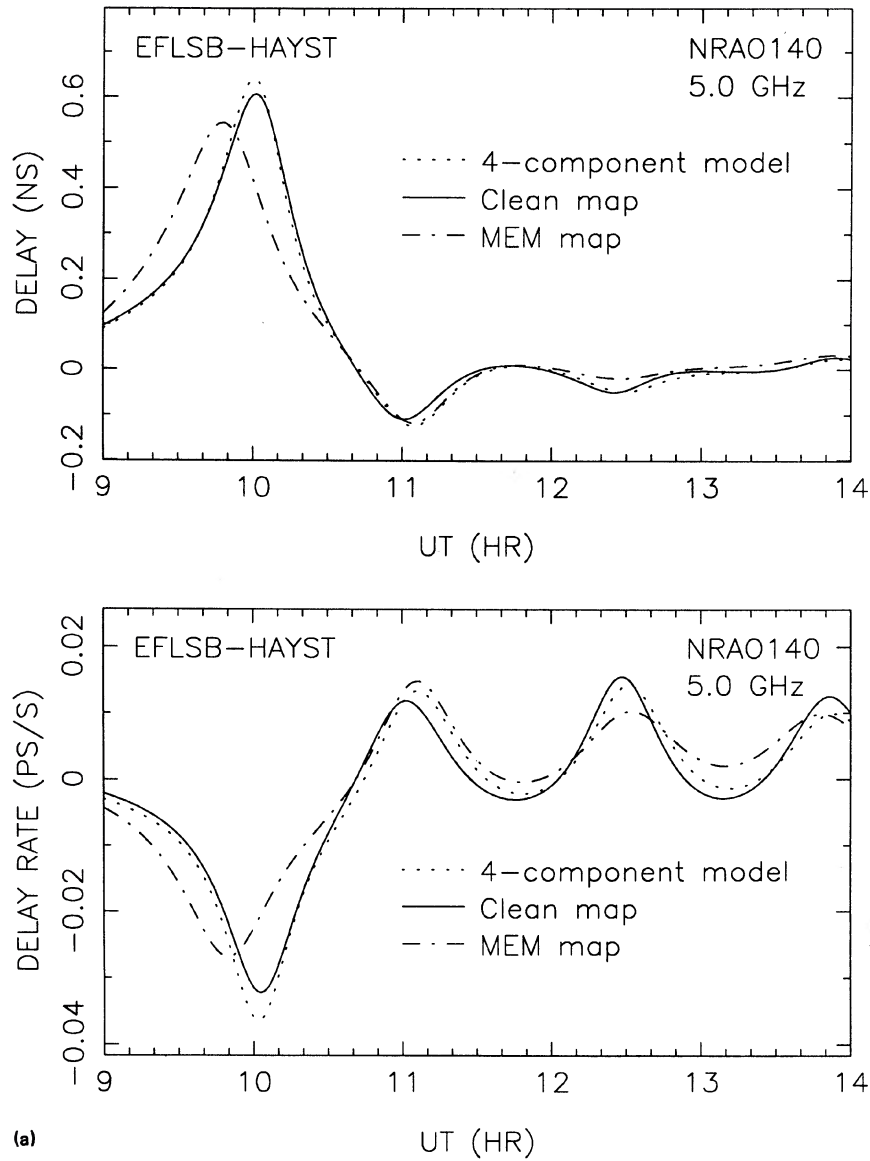
Fig. 4. Comparison of the structure effects at 5 GHz derived from the CLEAN map, the MEM map, and the four-component model of NRAO140 for the period of our observations. (a) baseline Effelsberg–Haystack; (b) baseline Effelsberg–VLA.

(a)
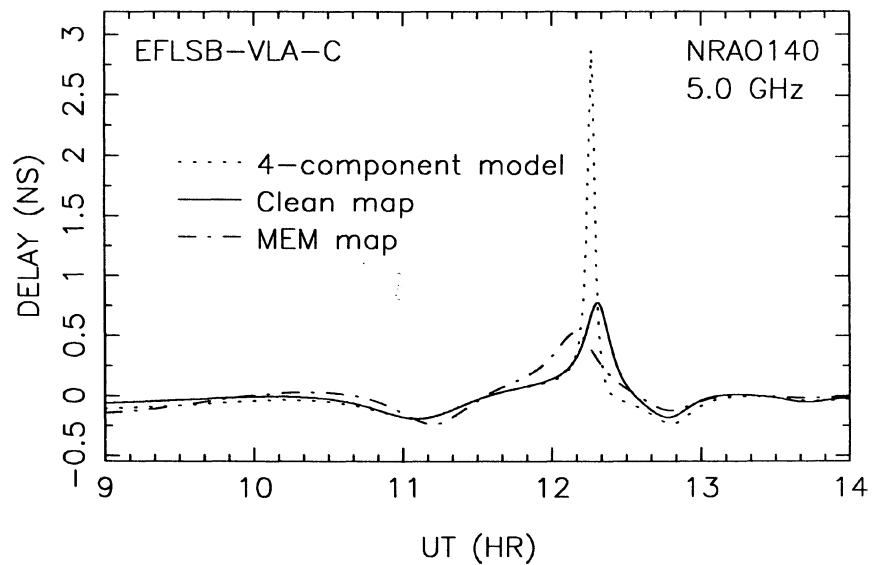
FIG. 4. (continued)
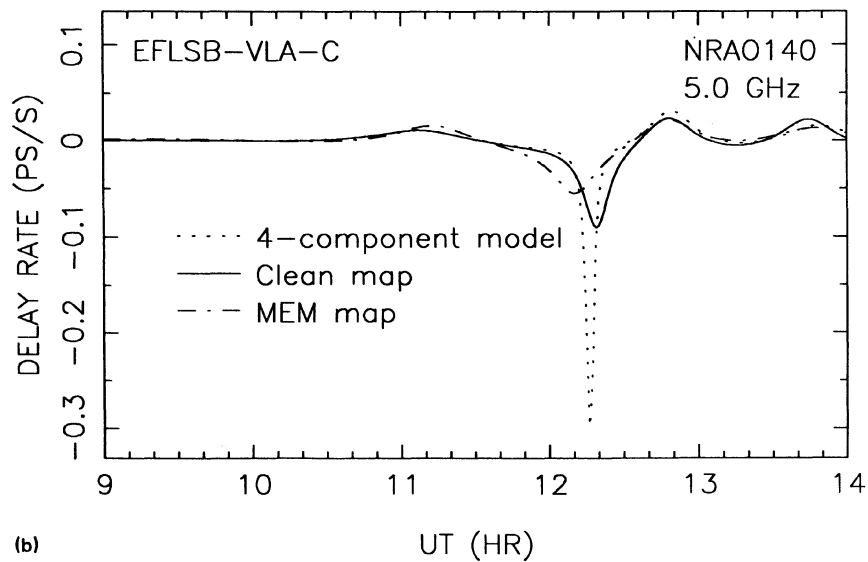
(b)
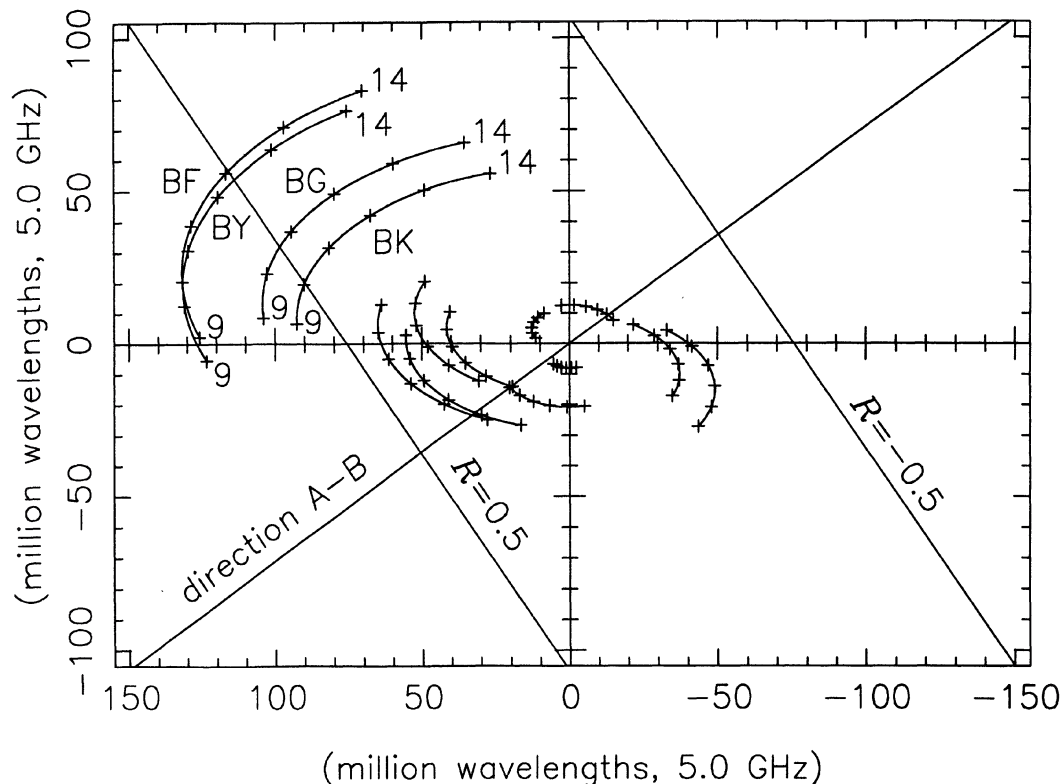
FIG. 5. u-v plane of NRAO140 with the direction of the axis joining the two main components A and B, and the straight line $R = \pm 0.5$ (R is the ratio between the separation of the components A and B and the projected interferometer fringe spacing along the direction A-B). The u-v tracks are plotted from 9 hr UT to 14 hr UT with crosses marked every hour. Intercontinental baselines are labeled by BK (Effelsberg–Haystack), BG (Effelsberg–Greenbank), BY (Effelsberg–VLA), and BF (Effelsberg–Fort Davis). The u-v track of the baseline Effelsberg–Owens Valley is not represented because it is very close to those of the baselines Effelsberg–VLA and Effelsberg–Fort Davis. Continental baselines are not labeled.

duced by the Gaussian model comes ~ 6 min after the one produced by the MEM map and ~ 2.5 min before the one produced by the CLEAN map. From examining the u-v tracks, it is possible to infer that a 6 min misregistration of the peaks for a two-component model is obtained when shifting the straight line $R = 0.5$ by $2.4 \times 10^6 \lambda$ along the source axis. Such a shift can be produced by a change of about 4% of the value of R, which means a change of 0.07 mas in the separation between components A and B. This change is consistent with the uncertainty quoted by CHL89 for this separation (± 0.05 mas). In addition, CHL89 noted that the separation between the brightness centroids of A and B is larger in the MEM map than in the CLEAN map with the latter being roughly equal to the one obtained with the four-component model. This is consistent with the fact that there is a better time coincidence between the peaks produced by the CLEAN map and the four-component model than there is with the MEM map (see Fig. 4). It is also understandable that the peaks produced by the MEM map appear first in time (Fig. 4) since the larger separation between A and B in this map makes the u-v tracks cross the straight line $R = 0.5$ earlier (see u-v plane in Fig. 5).

c) Comparison between the Measured and Calculated Structure Effects of NRAO140

Which representation (CLEAN map, MEM map, or four-component model) produces the most accurate astrometric

structure corrections for the BWS delays and delay rates of NRAO140? A useful test is to compare the closure delays and delay rates measured and calculated around triangles of baselines. These closure quantities depend on the structure of the source only. They are always null for a point source, while they depart from zero for a spatially extended source, similar to the closure phases used in hybrid mapping. For NRAO140, the closure BWS delays and delay rates measured during the July 1983 experiment exhibit significant departures from zero on intercontinental baselines (> 0.5 ns and > 0.1 ps/s, respectively), whereas they are comparatively smaller on continental U.S. baselines (< 0.5 ns and < 0.03 ps/s, respectively). These measured closure quantities have been compared to the corresponding closure structure corrections calculated from the CLEAN map, the MEM map, and the four-component model of NRAO140. Since the measured closure delays and delay rates are from the same dataset as the closure phases used to map NRAO140, these observables are not independent and the present comparison could be viewed only as a test of the consistency of our algorithm. However, not only the measured closure phases but also the measured amplitudes have been used to map NRAO140 by the three VLBI imaging techniques mentioned above, which introduces some degree of independence. A self-consistency test was actually carried out by calculating the structure closure phases from the brightness distributions and by comparing them with the observed closure phases originally used to make the maps. This test gave
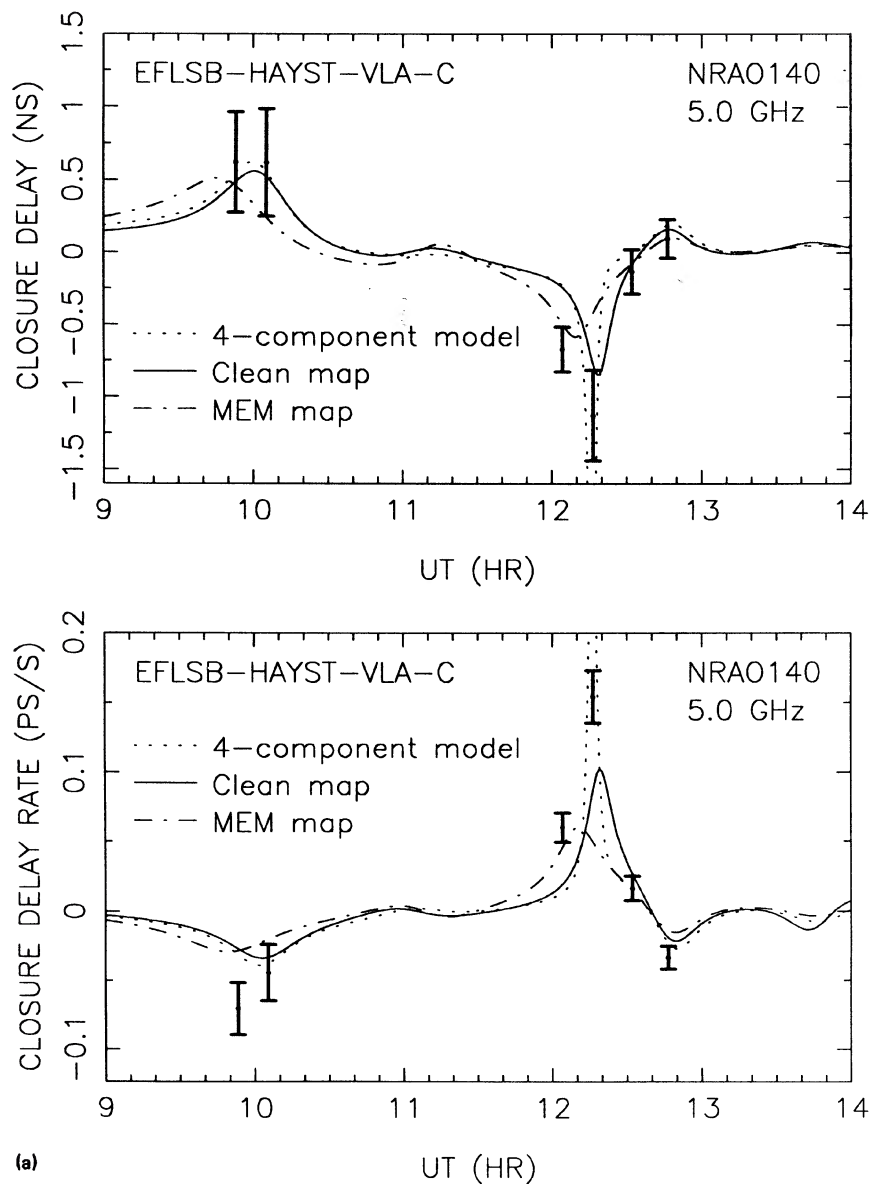
FIG. 6. Comparison of measured closure quantities (vertical bars) and calculated closure quantities derived from the CLEAN map, the MEM map, and the four-component model of NRAO140 (continuous curves): (a) triangle Effelsberg–Haystack–VLA; (b) triangle Greenbank–Effelsberg–VLA; (c) triangle Fort Davis–Effelsberg–VLA; (d) triangle Effelsberg–VLA–Owens Valley.

(b)
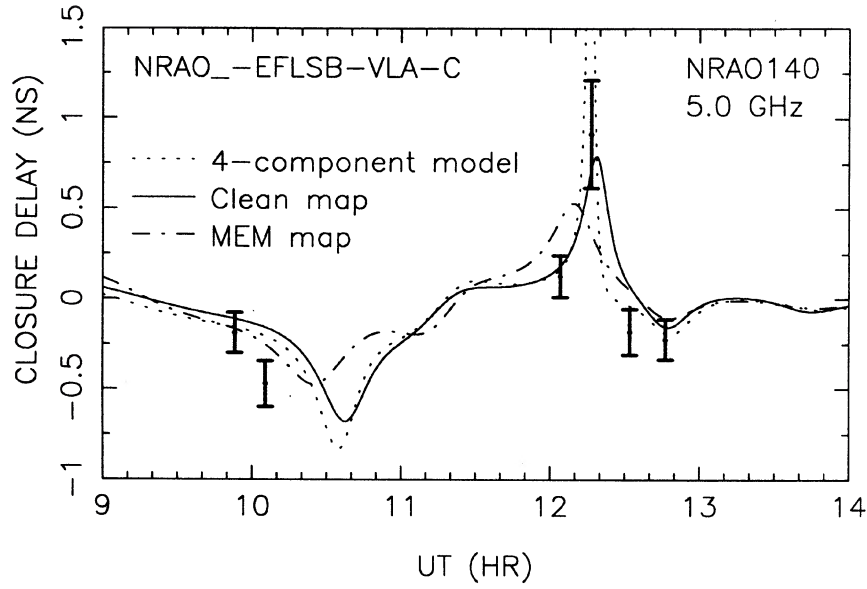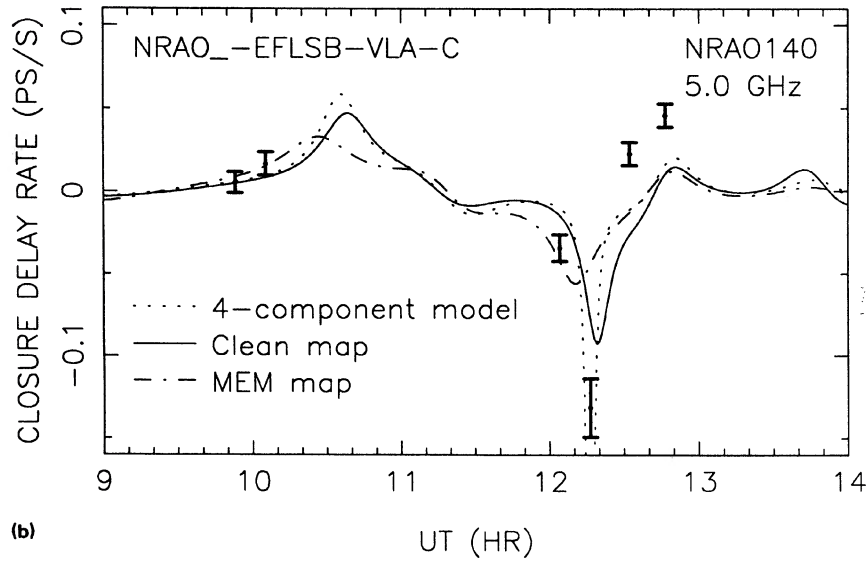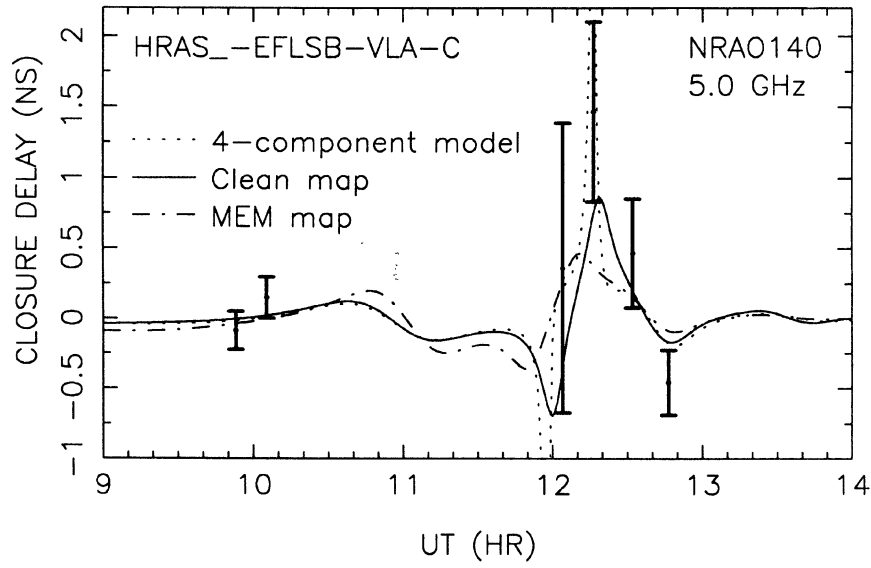
FIG. 6. (continued)

FIG. 6. (continued)

(d)
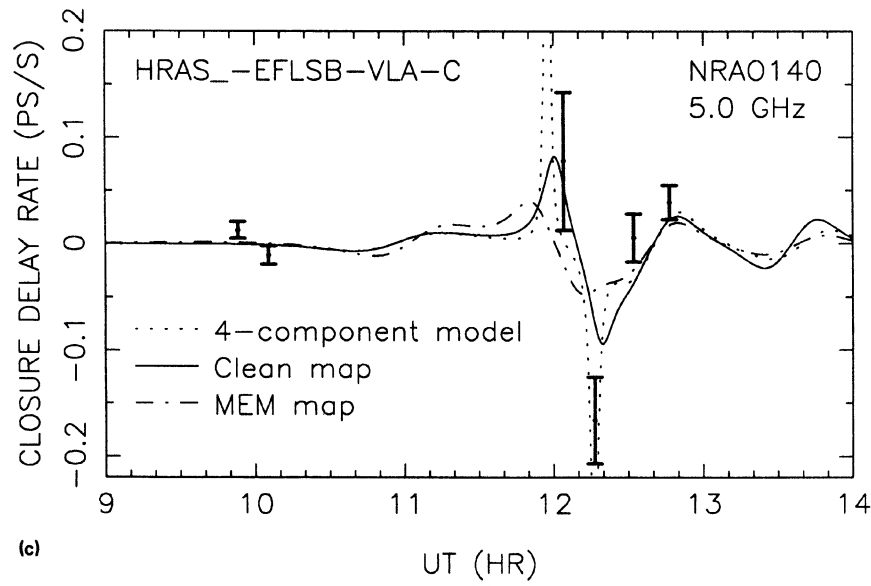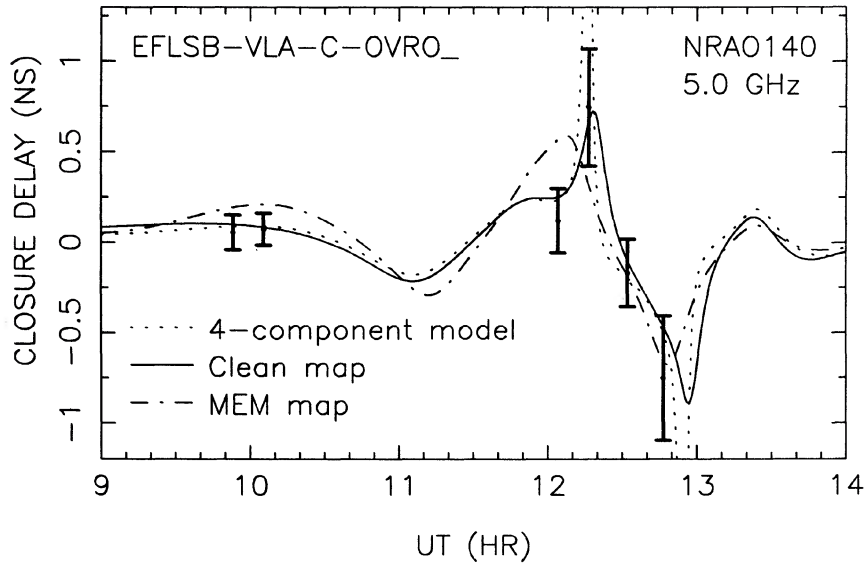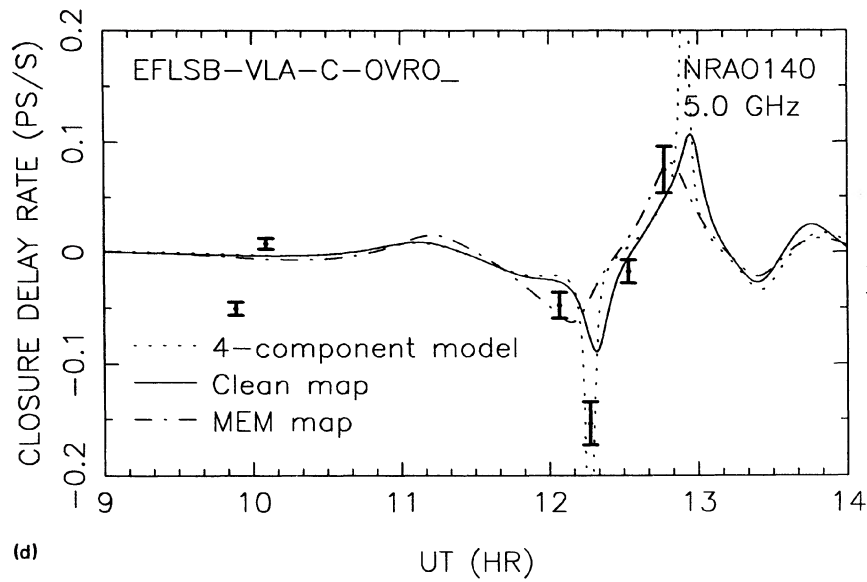
very consistent observed and calculated values for all the phases of the experiment. Although BWS delays and delay rates are frequency and time derivatives of the phases, likely systematic errors in the phases degrading the quality of the maps would not produce consistent biases in these derivatives. In addition, the fact that the three representations of the brightness distribution lead to structure corrections significantly different in some regions of the u-v plane implies that these structure corrections do not agree with the data at the same level. Thus, the test described here is an empirical approach to select the map that produces the structure corrections closest to the data.

Figures 6(a)–6(d) show examples of the comparison between the measured and calculated closure delays and delay rates of NRAO140 on four different intercontinental triangles of baselines. In these figures, it is noticeable that the observations made at the epochs of the peaks have uncertainties larger than those made at epochs where the structure effects are smaller. This is consistent with the fact that structure effects are maximum in regions where the visibility function is minimum and hence where the signal-to-noise ratio is also minimum. In Fig. 6, the peaks produced by the CLEAN map and the four-component model are approximately time registered with the departures from zero observed in the data but the peaks produced by the MEM map are shifted by a few minutes when compared to the data. The peak intensities appear to be correctly estimated in the case of the CLEAN map, though possibly slightly underestimated for the delay rate, whereas they are strongly overestimated in the case of the four-component model and significantly underestimated (at least 30%), especially for the delay rate, in the case of the MEM map. Therefore, the best agreement between measured and calculated closure quantities is obtained when structure corrections are calculated from the CLEAN map. In fact, computing the root-mean-square (rms) of the differences between the measured and calculated closure delays and delay rates of NRAO140 for all intercontinental triangles of baselines, shows that the CLEAN map leads to the smallest rms for both delay and delay rate (see Table I), and confirms this finding. Based on the empirical test described here, we argue that the CLEAN map of NRAO140 provides the most accurate structure corrections. Further investigations for other sources are necessary to infer whether or not one of the three representations (CLEAN map, MEM map, Gaussian component model) is definitely more appropriate for correcting structure effects in BWS delays and delay rates.

V. CONCLUSIONS

Radio-source structure effects in VLBI astrometric and geodetic measurements can be directly modeled in delay and delay rate when the brightness distributions of the sources are known. These effects are significant: for BWS delays, they are typically at a level of 0.1 ns and are sometimes larger than 1 ns (Charlot, Lestrade, and Boucher 1988). Many radio sources are reducible to a two-component model and a numerical simulation in this case provides general insights. Such a simulation shows that the closer the flux densities of the two components are, the larger the structure effects are. However, in the case of nearly equal flux densities, it is unlikely that these effects can be properly modeled because the dynamic range of the map of the brightness distribution would need to be extraordinarily high (for example, equivalent to a few 0.01% in the separation of the two compo-

TABLE I. Root-mean-square of the differences between the measured and calculated closure delays and delay rates of NRAO140 on ten intercontinental triangles of baselines.

	CLEAN map	MEM map	Four-component model
Delay (ns)	0.379	0.385	0.500
Delay rate (ps/s)	0.034	0.043	0.048

nents). This precision is not obtainable with existing VLBI mapping techniques. On the contrary, when the flux density ratio of the two components is 0.5 or below, a precision of 5% or less is required to model the BWS delay structure effect at the 10 ps level, and this can be obtained with the hybrid-mapping technique.

For NRAO140, the structure effects have been estimated by using three representations of the brightness distribution obtained with different VLBI mapping algorithms (the hybrid-CLEAN algorithm, the maximum entropy method, and model fitting). The comparison of the structure corrections calculated by these three representations indicates that they are consistent within 20%, provided the position of the projected baseline in the u-v plane is not close to regions of null visibilities. In the vicinity of null visibilities, calculated structure corrections exhibit very large peaks whose intensity and occurrence in time depend strongly on the map parameters. This was expected since NRAO140 consists mainly of two nearly equal components (A and B), and in this case, the structure effects at the epochs of the peaks (i.e., in low visibility regions of the u-v plane) are very difficult to model. The number of observations in the vicinity of null visibilities should be limited by proper scheduling in high-precision astrometry and geodesy. For NRAO140, the CLEAN map provides the best agreement between the measured and calculated structure closure delays and delay rates in these regions of the u-v plane. From this single example, however, it is not possible to say if this is a general statement. In the future, improvements of mapping techniques and use of larger VLBI arrays (e.g., the Very Long Baseline Array) should yield more accurate maps and therefore more accurate structure corrections in the low visibility regions of the u-v plane.

A stable VLBI celestial reference frame with a sub-milliarcsecond precision will require structure corrections of the BWS delays and delay rates measured in astrometry and geodesy. Therefore, a systematic program to monitor radio-source structures at both 2.3 and 8.4 GHz should be developed. It has been recently shown that geodetic experiments like those of the Crustal Dynamics Program can produce high-quality hybrid maps and can be used for this purpose (Charlot 1989, 1990). An alternative approach is to find the proper parametrization for modeling structure effects in the BWS delay and delay rate in order to directly estimate source structure parameters from the least-square fit of the astrometric and geodetic VLBI data. This would avoid the difficult task of producing a lot of maps and would be particularly valuable for differential VLBI measurements, for example for deep space tracking of spacecrafts in local reference frames, because the error budget is dominated by the source structure effects in this case (Treuhaft 1988).

to G. Petit and C. Boucher for useful discussions and for their support, to O. J. Sovers, R. N. Treuhaft, and C. Edwards for their comments, and to C. Ma for initial encouragement. He thanks all the participant observatories (Bonn, Haystack, NRAO–Greenbank, NRAO–VLA, Fort Davis, Owens Valley) for providing the high-quality data analyzed in this report, and especially the Haystack Observatory for correlating the observations. The author acknowledges the receipt of a BDI grant from the Centre National de la Recherche Scientifique and the Institut Géographique National to carry out this research. A portion of this work was performed at the Jet Propulsion Laboratory, California Institute of Technology, under contract with the National Aeronautics and Space Administration, while the author held a Lavoisier fellowship from the French Ministère des Affaires Etrangères.

REFERENCES

Bartel, N., Herring, T. A., Ratner, M. I., Shapiro, I. I., and Corey, B. E. (1986). Nature **319**, 733.

Campbell, J., Schuh, H., and Zeppenfeld, G. (1988). In *The Impact of VLBI on Astrophysics and Geophysics*, IAU Symposium No. 129, edited by M. J. Reid and J. M. Moran (Reidel, Dordrecht), p. 427.

Carter, W. E., Robertson, D. S., and Fallon, F. W. (1989). IERS Tech. Note 2, 35.

Charlot, P. (1989). Thèse de Doctorat de l'Observatoire de Paris, Paris, France.

Charlot, P. (1990). Astron. Astrophys. **229**, 51.

Charlot, P., Hough, D. H., and Lestrade, J.-F. (1989). Astron. Astrophys. **211**, 261 (CHL89).

Charlot, P., Lestrade, J.-F., and Boucher, C. (1988). In *The Impact of VLBI on Astrophysics and Geophysics*, IAU Symposium No. 129, edited by M. J. Reid and J. M. Moran (Reidel, Dordrecht), p. 33.

Coates, R. J., Clark, T. A., Counselman, C. C., Shapiro, I. I., Hinteregger, H. F., Rogers, A. E. E., and Whitney, A. R. (1975). Tectonophysics **29**, 9.

Cornwell, T. J., and Wilkinson, P. N. (1981). Mon. Not. R. Astron. Soc. **196**, 1067.

Cotton, W. E. (1979). In *Radio Interferometry Techniques for Geodesy*, NASA Conference No. 2115 (NASA Scientific and Technical Information Office, Springfield, Virginia), p. 193.

Davis, J. L., Herring, T. A., and Shapiro, I. I. (1988). In *The Impact of VLBI on Astrophysics and Geophysics*, IAU Symposium No. 129, edited by M. J. Reid and J. M. Moran (Reidel, Dordrecht), p. 367.

Dulk, G. A. (1985). Annu. Rev. Astron. Astrophys. **23**, 169.

Fujishita, M. (1983). Publ. Int. Latitude Obs. Mizusawa **XVII**, 13.

Kellermann, K. I., and Pauliny-Toth, I. I. K. (1981). Annu. Rev. Astron. Astrophys. **19**, 373.

Lestrade, J.-F., Mutel, R. L., Preston, R. A., and Phillips, R. B. (1985). In *Radio Stars*, edited by R. M. Hjellming and D. M. Gibson (Reidel, Dordrecht), p. 275.

Ma, C., Himwich, W., and Caprette, D. (1989). IERS Tech. Note 2, 1.

Ma, C., Ryan, J. W., and Caprette, D. (1989). NASA Technical Memorandum 100723.

Marscher, A. P. (1988). Astrophys. J. **334**, 552.

Marscher, A. P., and Broderick, J. J. (1982). Astrophys. J. Lett. **255**, L11.

Marscher, A. P., and Broderick, J. J. (1985). Astrophys. J. **290**, 735.

Pearson, T. J., and Readhead, A. C. S. (1984). Annu. Rev. Astron. Astrophys. **22**, 97.

Readhead, A. C. S., and Wilkinson, P. N. (1978). Astrophys. J. **223**, 25.

Rogers, A. E. E., Cappallo, R. J., Hinteregger, H. F., Levine, J. I., Nesman, E. F., Webber, J. C., Whitney, A. R., Clark, T. A., Ma, C., Ryan, J., Corey, B. E., Counselman, C. C., Herring, T. A., Shapiro, I. I., Knight, C. A., Shaffer, D. B., Vandenberg, N. R., Lacasse, R., Mauzy, R., Rayhrer, B., Schupler, B. R., and Pigg, J. C. (1983). Science **219**, 51.

Sovers, O. J. (1989). Private communication.

Sovers, O. J., Edwards, C. D., Jacobs, C. S., Lanyi, G. E., and Treuhaft, R. N. (1989). IERS Tech. Note 2, 25.

Tang, G., and Rönnäng, B. (1988). In *The Impact of VLBI on Astrophysics and Geophysics*, IAU Symposium No. 129, edited by M. J. Reid and J. M. Moran (Reidel, Dordrecht), p. 431.

Thomas, J. B. (1980). NASA–JPL Publ. **80–84**.

Treuhaft, R. N. (1988). TDA Prog. Rep. **42–94** (Jet Propulsion Laboratory, Pasadena, CA), p. 1.

Treuhaft, R. N., and Lanyi, G. E. (1987). Radio Sci. **22**, 251.

Ulvestad, J. S. (1988). In *The Impact of VLBI on Astrophysics and Geophysics*, IAU Symposium No. 129, edited by M. J. Reid and J. M. Moran (Reidel, Dordrecht), p. 429.